

**Ion-induced damage accumulation and electron-beam-enhanced recrystallization in SrTiO<sub>3</sub>**Y. Zhang,<sup>1,\*</sup> J. Lian,<sup>2</sup> C. M. Wang,<sup>1</sup> W. Jiang,<sup>1</sup> R. C. Ewing,<sup>2</sup> and W. J. Weber<sup>1</sup><sup>1</sup>*Pacific Northwest National Laboratory, P.O. Box 999, Richland, Washington 99352, USA*<sup>2</sup>*Department of Geological Sciences, University of Michigan, Ann Arbor, Michigan 48109, USA*

(Received 8 June 2005; published 21 September 2005)

Damage accumulation in strontium titanate (SrTiO<sub>3</sub>) from 1.0 MeV Au irradiation has been investigated at temperatures from 150 to 400 K. The relative disorder on the Sr and Ti sublattices at the damage peak has been determined as a function of local dose and temperature. A disorder accumulation model has been fit to data from this study and from the literature, indicating that defect-stimulated amorphization is the primary amorphization mechanism up to ~360 K. High-dose irradiation at 400 K leads to formation of an amorphous surface layer. Analyses of the temperature dependence for amorphization indicate that the amorphization kinetics are consistent with irradiation-enhanced and thermal recovery processes with activation energies of  $0.1 \pm 0.05$  eV and  $0.7 \pm 0.1$  eV, respectively. Under 200 keV electron-beam irradiation, the epitaxial recrystallization rates are orders of magnitude higher than thermal rates, and an activation energy of  $0.1 \pm 0.05$  eV is determined for the e-beam enhanced recrystallization processes.

DOI: [10.1103/PhysRevB.72.094112](https://doi.org/10.1103/PhysRevB.72.094112)

PACS number(s): 61.80.Fe, 68.37.Lp, 81.10.Jt

**I. INTRODUCTION**

Single crystal strontium titanate (SrTiO<sub>3</sub>) is of important technological interest in the microelectronics industry due to its high dielectric constant, good magnetic, ferroelectric and insulating properties, outstanding wear resistance, high resistance against oxidation, and high chemical and thermal stabilities.<sup>1-4</sup> Strontium titanate thin films are used as insulating layers in dynamic random access memories,<sup>2</sup> ferroelectric thin film structures,<sup>5</sup> and high- $T_c$  superconductor devices,<sup>6</sup> as well as potential gate oxide candidates.<sup>7</sup> In addition to advanced technological applications, titanate-based perovskites<sup>8,9</sup> and ceramics<sup>10</sup> are proposed as possible ceramic host phases for the immobilization of actinide and fission-product wastes. In many of these applications, knowledge of damage accumulation, dynamic recovery, and nanostructure evolution is critical. As a typical ABO<sub>3</sub> perovskite with the simple cubic structure at temperatures above 110 K, SrTiO<sub>3</sub> is chosen as a model perovskite for studying ion-induced damage accumulation and electron-beam-enhanced recrystallization in the current work.

For immobilization of nuclear waste, alpha decay of actinide elements produces high-energy alpha particles and low-energy heavy recoil nuclei (alpha recoils).<sup>8</sup> The alpha recoils account for most of the crystal damage produced through elastic scattering collisions. As a result, radiation damage accumulates in the titanate host phases and ultimately compromises the physical and chemical durability. Thus, it is important to understand and predict the behavior of the materials in a radiation environment. Since the peak in nuclear stopping for heavy ions, such as Au, is similar to the nuclear stopping of alpha recoils, the damage evolution at the damage peak under heavy-ion irradiation provides a reasonable simulation of the damage evolution behavior due to alpha-recoil collision cascades. Quantitative characterization of damage accumulation as a function of dose, temperature, and dose rate should lead to better understanding and predictive models of damage evolution, amorphization, dynamic

defect recovery, and dynamic recrystallization processes.

Previous studies of SrTiO<sub>3</sub> subjected to ion beam irradiation have included irradiation-induced epitaxial regrowth due to irradiation with He<sup>+</sup>, Ne<sup>+</sup>, Ar<sup>+</sup>, and Si<sup>+</sup> ions,<sup>3,11</sup> surface modification from 30 keV Ga<sup>+</sup> ions,<sup>12</sup> and damage accumulation<sup>13-15</sup> and recrystallization<sup>16-18</sup> from Kr<sup>+</sup>, Xe<sup>+</sup>, Au<sup>2+</sup>, and Pb<sup>2+</sup> ions. A number of studies have been carried out to characterize the critical dose for amorphization,<sup>13-15</sup> but only a few studies have quantitatively investigated the damage evolution as a function of both dose and temperature.<sup>15</sup> In the present study, the temperature dependence of damage accumulation under Au ion irradiation is investigated, and the results are discussed in comparison with other studies, including the effects of dose rates.<sup>13-15</sup> A disorder accumulation model,<sup>19,20</sup> which is remarkably different from that applied previously,<sup>15</sup> is fit to the experimental data. In addition, the response of the ion-beam-induced amorphous layers to electron beam (e-beam) irradiation is investigated.

**II. EXPERIMENTAL PROCEDURE**

The high-purity single crystal SrTiO<sub>3</sub> samples used in this study were obtained from Princeton Scientific Corp. (NJ). The crystals were epipolished with dimensions of 10 mm × 10 mm × 1 mm and oriented along the [100] axis.

Irradiation of SrTiO<sub>3</sub> with 1.0 MeV Au<sup>+</sup> or Au<sup>2+</sup> ions and subsequent investigation of damage analysis based on ion channeling methods were carried out using the 3.0 MV tandem accelerator facilities within the Environmental Molecular Sciences Laboratory (EMSL) at the Pacific Northwest National Laboratory (PNNL). The crystals were mechanically mounted to a molybdenum plate using molybdenum spring-loaded clips, with a Chromel-Alumel thermocouple clamped to the sample surface. The crystals were irradiated at ion fluxes in the range of  $1.2 \times 10^{12}$ – $1.7 \times 10^{12}$  cm<sup>-2</sup> s<sup>-1</sup> over temperatures from 150 to 400 K to ion fluences from  $2 \times 10^{12}$  to  $6.0 \times 10^{15}$  cm<sup>-2</sup>. A large tilt angle of 60° relative

to the surface normal was used to produce shallow damage that could be readily measured by Rutherford backscattering spectrometry (RBS) in channeling geometry.<sup>21</sup> After each irradiation, the crystal was kept under high vacuum ( $\sim 10^{-7}$  Torr) in the target chamber, and RBS with 2.0 MeV He<sup>+</sup> beam was performed *in situ*, along both the  $\langle 100 \rangle$ -axial direction and an off-channel (random) direction, with a Si detector located at a scattering angle of  $150^\circ$  relative to the incoming beam. For the irradiation at 150 K, the RBS analyses were carried out at 150 K. For room temperature and higher temperature irradiation, the RBS analyses were performed at room temperature to effectively quench any thermal recovery processes prior to analysis. No significant disordering contributions from the He<sup>+</sup> analysis beam were observed in this study. At each ion fluence, the local dose at the damage peak, in displacements per atom (dpa), was determined using SRIM 2003.20 full-cascade simulations<sup>22,23</sup> under the assumptions of a sample density of  $5.118 \text{ g cm}^{-3}$  ( $8.4 \times 10^{22} \text{ at cm}^{-3}$ ) and threshold displacement energies of 45, 70, and 80 eV for O,<sup>24,25</sup> Ti,<sup>26</sup> and Sr,<sup>26</sup> respectively. Using the SRIM results for the average number of displaced atoms per unit length per incident ion as a function of depth, the conversion factor at the damage peak from ion fluence to dose (dpa) is  $0.655 \times 10^{-14} \text{ dpa cm}^2$ , which is derived from the SRIM result at the damage peak divided by the atomic density. These same parameters and SRIM program were used to calculate the conversion factor and local dose for data from other studies<sup>14,15</sup> for comparison.

For the study of electron-beam-enhanced recrystallization, amorphous surface layers were formed in SrTiO<sub>3</sub> by 1.0 MeV Au irradiation at 400 K to high fluences. The microstructural features, electron diffraction patterns, high-resolution transmission electron microscopy (TEM) images, and recrystallization rates of the samples were determined at 300, 353 and 393 K using a JEOL 2010F TEM at the University of Michigan (UM) operated at 200 kV. Cross-sectional TEM samples were prepared by the wedge technique using a tripod polisher. Specimens were prepared by pure mechanical polishing, which was followed by ion milling using 4 keV Ar<sup>+</sup> to obtain thin areas suitable for TEM observations. Ion milling may induce point defects or create a surface amorphous layer with a thickness of several nm on the thin areas of the TEM samples. However, this surface amorphous layer is much smaller than the typical sample thickness required for high-resolution TEM imaging, and should not have significant effects on the original damage profile induced in SrTiO<sub>3</sub> by high energy Au ions.

### III. RESULTS AND DISCUSSION

#### A. Disorder accumulation model

The irradiation-induced relative disorder,  $S$ , measured by ion-channeling techniques contains contributions from amorphous domains, interstitials, interstitial clusters and extended defects, as given by the expression,<sup>19,20</sup>

$$S = f_a + S_d + S_c, \quad (1)$$

where  $f_a$  is the amorphous fraction,  $S_d$  is the relative disorder contribution from interstitials and small interstitial clusters in

the residual crystalline material, and  $S_c$  accounts for the relative disorder from the evolution of extended defect clusters, which is negligible except near the critical temperature for amorphization and is not included in the present model fits. There have been several models<sup>27</sup> applied by different groups to describe defect accumulation and amorphization. The Hecking model,<sup>28</sup> which is based on two coupled differential equations, has been used to describe the rate of disordering in semiconductors; however, it is not easily fit to experimental data. An analytical solution to the amorphization rate within the Hecking model has been provided in a review of amorphization models and mechanisms.<sup>27</sup> This analytical solution for the amorphous fraction, where amorphization occurs both directly within a cascade and from defect-stimulated processes, has been referred to as the direct-impact/defect-stimulated (DI/DS) model and is given by the expression<sup>27</sup>

$$f_a = 1 - (\sigma_a + \sigma_s) / \{ \sigma_s + \sigma_a \exp[(\sigma_a + \sigma_s)D] \}, \quad (2)$$

where  $\sigma_a$  is the amorphization cross section,  $\sigma_s$  is the effective cross section for defect-stimulated amorphization, and  $D$  is the local dose. The disorder from irradiation-induced interstitials and small interstitial clusters is described by a simple defect accumulation model<sup>29</sup> and is given by the expression<sup>19,20</sup>

$$S_d = S_d^* [1 - \exp(-BD)] (1 - f_a), \quad (3)$$

where  $S_d^*$  is the saturation value for the defect-induced disorder and  $B(\text{dpa}^{-1})$  is proportional to an effective recombination volume for the specific defects giving rise to  $S_d$ .

#### B. Temperature dependence of damage accumulation

The RBS spectra of samples under 1.0 MeV Au<sup>2+</sup> irradiation were measured along the  $\langle 100 \rangle$  direction from 150 K to 400 K. In this study, an iterative procedure<sup>30-32</sup> is applied to each RBS channeling spectrum to determine the dechanneling component for both the Sr and Ti sublattices, which enables the relative disorder on the Sr and Ti sublattices to be determined from the RBS channeling spectra using the ratio of aligned spectra to random spectra after correcting for the background-dechanneling fraction.<sup>19,20</sup> A continuous buried amorphous state is defined as achieving a relative disorder of 1.0 over some incremental depth, where the resulting aligned backscattering yield coincides with the random level.

The relative disorder on the Sr and Ti sublattices at the damage peak for the samples irradiated at different temperatures is shown in Fig. 1. A sigmoidal dependence of damage accumulation on dose is observed at all irradiation temperatures and on both sublattices. The disorder accumulation model [Eq. (1)], which has been successfully applied to several materials over a range of irradiation conditions,<sup>19,20,33,34</sup> is fit to the damage accumulation data in SrTiO<sub>3</sub> at 150 K though 360 K in the current study, with  $S_c$  assumed to be negligible at these temperatures. The parameters are summarized in Table I. For all irradiation temperatures, the significantly larger values of  $\sigma_s$  relative to  $\sigma_a$  indicate that defect-stimulated amorphization is the primary mechanism that

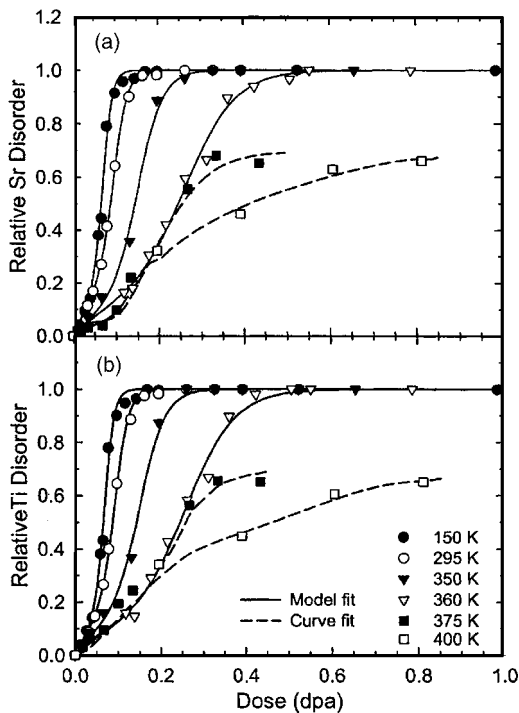


FIG. 1. Relative disorder at the damage peak on Sr and Ti sublattices as a function of local dose for  $\text{SrTiO}_3$  single crystals irradiated with 1.0 MeV Au ions at temperatures from 150 to 400 K. The uncertainty for each data point is  $\sim 4\%$ . The solid lines are the fits of Eq. (1) to the data at 150, 295, 350 and 360 K, and the model parameters are summarized in Table I. The dashed lines are smooth curve fits to the data at higher temperatures to guide the eye.

leads to the growth of amorphous nuclei and coalescence of amorphous domains. Similar cross sections,  $\sigma_a$  and  $\sigma_s$ , for both Sr and Ti sublattices indicate that the amorphous state is essentially stoichiometric. The same  $B$  values for the Sr and Ti sublattices are expected, since close-pair recombination kinetics are expected to be similar.

When ion implantation is performed at a relatively high temperature, dynamic recovery processes, including defect migration and clustering, become more active. Slight changes in the irradiation temperature can dramatically affect the recovery rates. As a result, the disorder accumulation becomes very sensitive to irradiation temperature, as shown in Fig. 1 for irradiations at temperatures above 295 K. Increasing irradiation temperature eventually leads to a condition where the damage production and recovery rates are

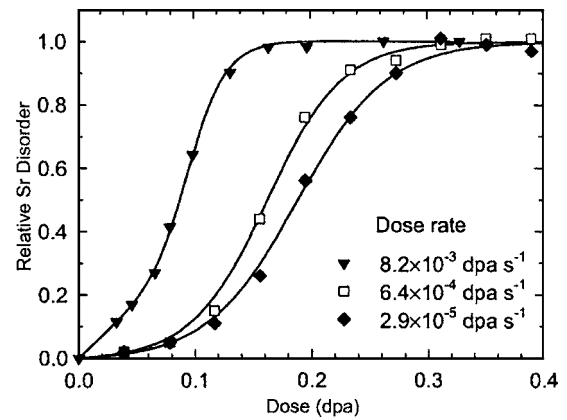


FIG. 2. Relative disorder at the damage peak on Sr sublattice as a function of local dose for  $\text{SrTiO}_3$  single crystals irradiated with 1.0 MeV  $\text{Au}^{2+}$  at 295 K with dose rate of  $8.2 \times 10^{-3} \text{ dpa s}^{-1}$ . The uncertainty for the data from this study is  $\sim 4\%$ . Also included are the damage accumulation curves on Sr sublattice due to Pb ion irradiation at room temperature from Ref. 15 with dose rates of  $6.4 \times 10^{-4}$  and  $2.9 \times 10^{-5} \text{ dpa s}^{-1}$ , respectively. The solid lines are the fits of Eq. (1) to the data, and the model parameters are summarized in Table I.

equal, which defines the conditions controlling the critical temperature for amorphization. At high irradiation temperatures ( $>360 \text{ K}$ ), significant dynamic recovery occurs; some irradiation-induced defects become highly mobile and agglomerate to form extended defect clusters [term  $S_c$  in Eq. (1)] that contribute to the total disorder.<sup>20</sup> Due to limited data and more complex behavior, the disorder accumulation model [Eq. (1)] has not been fit to the high temperature data where the contributions of the extended defect clusters [term  $S_c$  in Eq. (1)] become important; however, a smooth curve fit to the data is provided as a guide.

### C. Dose-rate effects on damage accumulation

The dose dependence of the relative Sr disorder accumulation at the damage peak for irradiation at 295 K is shown in Fig. 2 for a dose rate of  $8.2 \times 10^{-3} \text{ dpa s}^{-1}$  (an ion flux of  $1.25 \times 10^{12} \text{ cm}^{-2} \text{ s}^{-1}$ ). For comparison, the damage accumulation data on the Sr sublattice,<sup>15</sup> due to 320 keV Pb ion irradiation at 295 K at two lower dose rates,  $6.4 \times 10^{-4}$  and  $2.9 \times 10^{-5} \text{ dpa s}^{-1}$  (corresponding to ion fluxes of  $1.65 \times 10^{11}$  and  $7.5 \times 10^9 \text{ cm}^{-2} \text{ s}^{-1}$ , respectively), are also included. The solid lines are fits of Eq. (1) to all the data, and

TABLE I. Model parameters from fits of Eq. (1) to data in Figs. 1 and 2. The uncertainty is  $\sim 10\%$  for  $\sigma_a$  and  $\sigma_s$ ,  $\sim 20\%$  for  $S_d^*$  and  $B$ .

Sublattice	150 K		295 K		350 K		360 K		295 K Sr Sublattice <sup>a</sup>	
	Sr	Ti	Sr	Ti	Sr	Ti	Sr	Ti	High flux	Low flux
$\sigma_a$ ( $\text{dpa}^{-1}$ )	0.2	0.2	0.2	0.2	0.2	0.2	0.2	0.2	0.2	0.2
$\sigma_s$ ( $\text{dpa}^{-1}$ )	85	86	59	60	33	33	17	17	31	26
$S_d^*$	0.4	0.3	0.4	0.3	0.2	0.2	0.1	0.1	0.01	0.001
$B$ ( $\text{dpa}^{-1}$ )	10	10	10	10	10	10	10	10	10	10

<sup>a</sup>Reference 15.

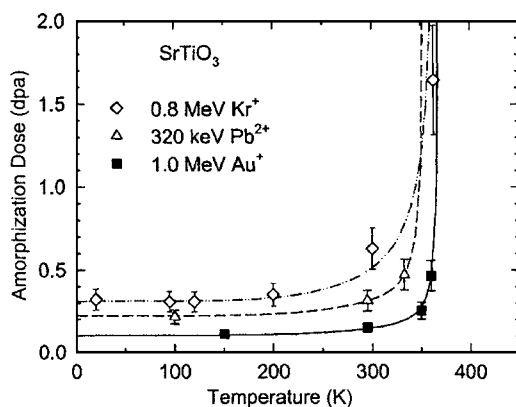


FIG. 3. Temperature dependence of the dose to achieve a relative disorder level of 0.97 in SrTiO<sub>3</sub> under 1.0 MeV Au irradiation, along with previous TEM results for amorphization dose under 800 keV Kr<sup>+</sup> and Xe<sup>+</sup> irradiations (Refs. 13 and 14) and ion channeling results from 320 keV Pb<sup>2+</sup> irradiations (Ref. 15). The lines are the model fits to the data.

the model parameters are included in Table I. The nonlinear dose dependence is clearly evident for all ion fluxes. The results in Fig. 2 demonstrate a strong dose-rate effect, as a much higher rate of disordering is observed with increasing ion flux. Full amorphization from the model fit is achieved at  $\sim 0.24$ , 0.47, and 0.55 dpa as the dose rate decreases from  $8.2 \times 10^{-3}$  to  $2.9 \times 10^{-5}$  dpa s<sup>-1</sup>. Because the rate of thermal recovery should be constant at the same temperature, the shift of the curves to higher doses at the lower dose rates indicates decreased damage accumulation rates due to larger effects of dynamic thermal recovery on damage accumulation kinetics, which is consistent with the temperature and dose rate dependent form of the DI/DS model.<sup>27</sup>

#### D. Temperature dependence of amorphization

For comparison with previous *in situ* TEM determinations<sup>13,14</sup> of the critical amorphization dose, the RBS critical dose for amorphization is defined in this study as the dose to achieve an amorphous fraction of 0.97 due to increasing uncertainty in defining the dose for complete amorphization as  $f_a$  approaches 1.0. The critical dose for amorphization is defined for each temperature based on model fits to the Sr data in Fig. 1(a), and the results are shown in Fig. 3 as a function of irradiation temperature. The amorphization doses from *in situ* TEM studies<sup>13,14</sup> for irradiation with 800 keV Kr<sup>+</sup> ions are also included in Fig. 3, together with the RBS results from the 320 keV Pb<sup>2+</sup> irradiations.<sup>15</sup>

A relationship between dose and temperature to achieve a specific amorphous state has been previously derived based on a temperature-dependent form of the DI/DS model for amorphization.<sup>27</sup> This model considers both epitaxial recrystallization,  $K_e(T)$ , and defect recombination/annihilation,  $K_d(T)$ , rates. Since epitaxial thermal recrystallization does not appear to play a significant role in the temperature dependence of amorphization in SrTiO<sub>3</sub>,<sup>16,17</sup> the dose required to achieve a specific amorphous state is given by the expression<sup>27</sup>

$$D = [D_0 + A \phi \ln\{1 - AK_d(T)\} \times [1 - \exp(-D_0/\phi A)]] / [1 - AK_d(T)], \quad (4)$$

where  $A = [\phi(\sigma_a + \sigma_s)]^{-1}$ ,  $\phi$  is the ion flux, and  $D_0$  is the dose to achieve the specific amorphous state at 0 K. As noted elsewhere,<sup>27</sup> the recovery rate in Eq. (4) is the sum of temperature-dependent rate constants for both irradiation-enhanced and thermal annealing processes [i.e.,  $K_d(T) = K_{irr}(T) + K_{th}(T)$ ], each with its own effective jump frequency and activation energy. The irradiation-enhanced recovery processes may be nearly athermal with low activation energies. The results of iterative fits of Eq. (4) to all data in Fig. 1 are indicated by the curves in Fig. 3, and the results yield activation energies of  $0.1 \pm 0.05$  eV and  $0.7 \pm 0.1$  eV for irradiation-enhanced and thermal recovery processes, respectively. The effective jump frequencies for irradiation-enhanced and thermal processes are on the order of 10 and  $10^9$  s<sup>-1</sup>, respectively.

The activation energy of  $0.1 \pm 0.05$  eV for irradiation-enhanced processes is similar to those previously measured for ion-beam-enhanced epitaxial recrystallization in SrTiO<sub>3</sub> (Ref. 3) and the same as that determined in the present study (below) for *e*-beam enhanced epitaxial recrystallization in SrTiO<sub>3</sub>, suggesting similar irradiation-enhanced processes related to defect recovery or epitaxial recrystallization. The activation energy of  $0.7 \pm 0.1$  eV for the thermal recovery process is consistent with the anion and cation thermal recovery stages previously observed below 350 K in SrTiO<sub>3</sub> irradiated with He and O ions,<sup>18</sup> as well as with the calculated activation energy of 0.65 eV for oxygen vacancy migration in SrTiO<sub>3</sub>.<sup>35</sup>

Considering the differences in defining the dose for amorphization by RBS and TEM techniques, the difference in sample geometries, the uncertainties in ion fluence measurements, and the effects of ion mass (lighter Kr<sup>+</sup> ions in the TEM experiments versus heavier Pb<sup>2+</sup> and Au<sup>2+</sup> ions in RBS measurements), the results in Fig. 3 indicate reasonable agreement between the two techniques. The difference between the Pb and Au data is primarily due to the more than two orders of magnitude lower ion flux in the case of the Pb irradiations, which suggests that damage-rate effects may be significant over a wide temperature range. The data and model fits in Fig. 3 clearly indicate that, under these irradiation and analysis conditions, the critical temperature for amorphization in SrTiO<sub>3</sub> is close to 370 K and controlled by thermal recovery processes. While amorphization does not occur at the damage peak above 370 K under these irradiation conditions, amorphization can still be induced at 400 K at the surface under these conditions (discussed below), where the surface affects the local balance of damage production and recovery.

Equation (2) above is an idealization of irradiation-induced amorphization without any consideration of the recovery kinetics. Equation (4) was derived from the kinetics dependent DI/DS model<sup>27</sup> that contains the dependence on temperature and dose rate. In this kinetics dependent DI/DS model, the cross section for defect-stimulated amorphization,  $\sigma_s$ , is replaced by the expression

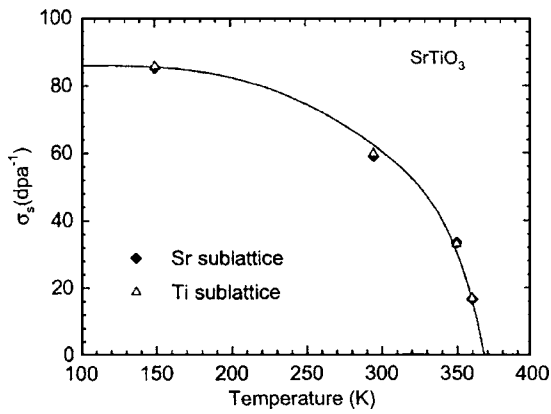


FIG. 4. Temperature dependence of the effective cross section for defect-stimulated amorphization ( $\sigma_s$ ) under 1.0 MeV Au irradiation. The solid lines are the fit of Eq. (5).

$$\sigma_s = \sigma_{s0} - K_d(T)/\phi, \quad (5)$$

where  $\sigma_{s0}$  is the defect-stimulated cross section at 0 K, and  $K_d(T)$  and  $\phi$  are as defined in Eq. (4). The temperature dependence of  $\sigma_s$  (from Table I) is shown in Fig. 4, along with a fit of Eq. (5). Based on these fitting parameters, the model fit yields a value of 86 dpa $^{-1}$  for  $\sigma_{s0}$  and activation energies of  $0.1 \pm 0.05$  eV and  $0.7 \pm 0.1$  eV for irradiation-enhanced and thermal recovery processes, respectively. The dynamic recovery kinetics affects not only amorphization, but also defect recovery and clustering. These results provide a consistent interpretation of the kinetics of amorphization and damage accumulation.

### E. Electron-beam-enhanced recrystallization

Irradiation with 1.0 MeV Au at 400 K results in a highly-damage surface layer. As the irradiation dose increases, an amorphous layer starts to form at the surface, instead of at the damage peak region, as observed at temperatures below 360 K. The amorphous layer thickness increases with the ion fluence. In this study, amorphous surface layers of two thickness were formed: sample A was irradiated to an ion fluence of  $6.0 \times 10^{15}$  cm $^{-2}$  at 60° off the surface normal with an ion flux of  $1.7 \times 10^{12}$  cm $^{-2}$  s $^{-1}$  to create an amorphous thickness of  $\sim 10$  nm and sample B was irradiated to a fluence of  $4.5 \times 10^{16}$  cm $^{-2}$  at 7° off the surface normal with an ion flux of  $3.5 \times 10^{12}$  cm $^{-2}$  s $^{-1}$  to create an amorphous thickness of  $\sim 330$  nm. During exposure of the amorphous layers to 200 keV e-beams within the TEM, the amorphous layer thickness decreases with exposure time (as shown in Fig. 5), indicating *in situ* epitaxial recrystallization at the amorphous/crystalline (*a/c*) interface under e-beam irradiation. Studies on the irradiation-induced amorphous-to-crystalline phase transition<sup>14,17,18,36–43</sup> and surface characterization<sup>1,44</sup> have shown that amorphous layers in SrTiO $_3$  can regrow under thermal annealing, and solid-state epitaxial recrystallization by thermal annealing in vacuum<sup>14,17,18,36–42</sup> can often initiate from the underlying crystalline substrate at temperatures above  $\sim 600$  K, far below the bulk melting point of the material.

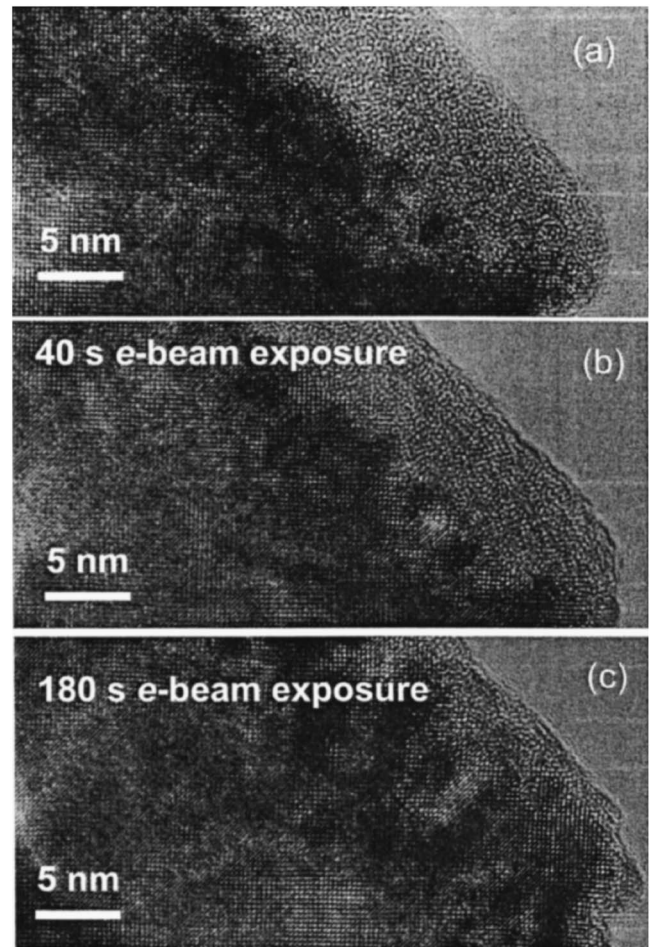


FIG. 5. High resolution TEM images of sample B showing the *a/c* interface motion under e-beam exposure with flux of  $5.0 \times 10^{20}$  cm $^{-2}$  s $^{-1}$ . A complete amorphous layer starting from the surface with the thickness of  $\sim 330$  nm was created in sample B by Au ion beam implantation. In this study, a much thinner amorphous layer was deliberately used for e-beam irradiation experiment by prolonging ion beam thinning during the sample preparation.

Since solid-phase epitaxial regrowth is often observed at elevated temperatures, an important consideration in the present study is the temperature increase due to the e-beam irradiation. Electron-beam annealing of amorphous regions has been studied in semiconductors<sup>45,46</sup> and observed in several oxides.<sup>41,47</sup> The temperature rise under different e-beam conditions can vary from a few K up to 40 K. The maximum temperature rise  $\Delta T$  associated with electron irradiation during TEM measurements can be calculated according to the following formula:<sup>41,48,49</sup>

$$\Delta T = \frac{I}{\pi \kappa e} \left( \frac{\Delta E}{d} \right) \ln \frac{b}{r_o}, \quad (6)$$

where  $I$  is the beam current,  $\kappa$  the thermal conductivity,  $b$  the sample radius,  $r_o$  the beam radius,  $e$  is the electron charge, and  $\Delta E$  is the total energy loss per electron in a sample of thickness  $d$ . Since the electron energy loss, normally a few eV/nm, is negligible as compared to the initial energy (200 keV),  $\Delta E/d$  is assumed to be constant and given by the

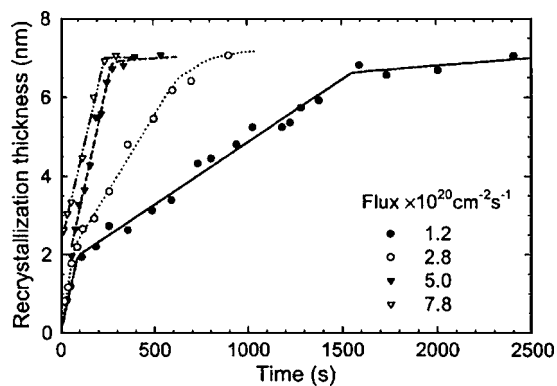


FIG. 6. Solid phase regrowth of amorphous-to-crystalline transition as a function of exposure time to the e-beam under different fluxes. The uncertainty for the data from this study is  $\sim 5\%$ . The e-beam irradiation was carried out at room temperature.

stopping power for the electrons,  $dE/dx$ , in  $\text{SrTiO}_3$ . It is worth noting that, although electron probes may involve a high current density, the temperature rise, as a result of the logarithmic term in Eq. (6), may be small. The thermal conductivities of perovskites vary from 6 to 11 W/mK at room temperature.<sup>50</sup> The maximum temperature rise for sample A with an electron flux of  $1.2 \times 10^{20} \text{ cm}^{-2} \text{ s}^{-1}$  is less than 3 K with  $I=6 \text{ nA}$ ,  $\kappa=6 \text{ W/mK}$ ,  $b=1.5 \text{ mm}$ ,  $r_0=100 \text{ nm}$ , and  $dE/dx(200 \text{ keV})=1 \text{ eV/nm}$ , which was calculated from the Bethe-Bloch equation<sup>49</sup> assuming a mean excitation energy of 249 eV.<sup>51</sup> The maximum temperature rise for sample B is below 8 K with  $I=14.1 \text{ nA}$ ,  $\kappa=6 \text{ W/mK}$ ,  $b=1.5 \text{ mm}$  and  $r_0$  varies between 60 and 100 nm for electron fluxes between 7.8 and  $2.8 \times 10^{20} \text{ cm}^{-2} \text{ s}^{-1}$ . The temperature increase due to e-beam heating is, therefore, negligible, which is in agreement with other studies.<sup>41,49,52</sup>

The *in situ* recrystallization of the amorphous layer is observed by TEM at room temperature under different beam fluxes, and is summarized in Fig. 6 by averaging the thickness of the amorphous layer from different locations. There is normally some density variation of the amorphous and recrystallized states. Recrystallization is a dynamical process, and the density in the recrystallized material may vary with the electron dose. The recrystallization rate is, therefore, based on decreases in the amorphous layer thickness. Although a nonuniform thickness of the amorphous layer is observed, the average thickness of the surface amorphous layer decreases during prolonged exposure to the e-beam. The solid phase regrowth shows a series of linear stages with decreasing slopes as the exposure time increases, resembling a sublinearlike regrowth behavior. In general, the recrystallization rates due to the e-beam irradiation can be separated into three stages, as shown by the slope changes in the low-flux curves ( $1.2$  and  $2.8 \times 10^{20} \text{ cm}^{-2} \text{ s}^{-1}$ ) in Fig. 6. During the initial stage, up to  $\sim 100 \text{ s}$ , there exist many ion-induced defects near the *a/c* interface. Rapid motion at the *a/c* interface is observed, and the recrystallization processes proceed at a high rate. This fast recrystallization may be attributed to e-beam enhanced defect annihilation at the *a/c* interface. Under the high e-beam flux ( $5.0$  and  $7.8 \times 10^{20} \text{ cm}^{-2} \text{ s}^{-1}$ ), the recrystallization processes during the initial stage occur rap-

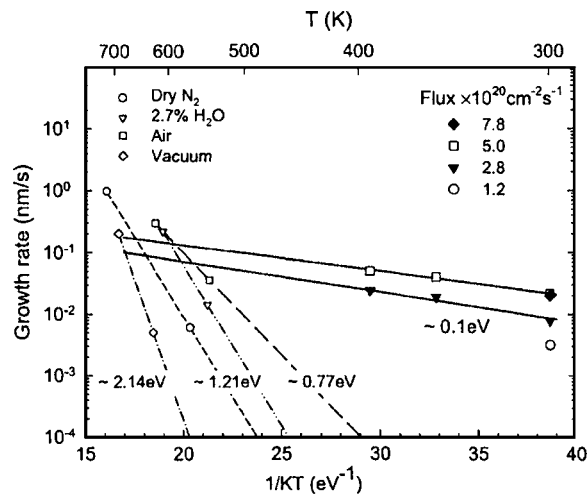


FIG. 7. Arrhenius plots for the solid phase regrowth. The recrystallization rate due to the e-beam induced regrowth is indicated by the solid lines. The uncertainty for the data from this study is  $\sim 5\%$ . Previous results (Refs. 36–38) are also included as dashed lines for comparison.

idly, and no data were obtained during the very short times. After the initial stage where most ion-induced defects are annealed out, the recrystallization rates are constant, which represents a second stage. A well-defined linear relationship is observed for different fluxes at this stage. At longer times, the mobility of the *a/c* interface slows down, and the recrystallization processes approach a saturation stage. The TEM observations indicate that the saturation stage occurs when the thickness of the remaining amorphous layer is  $\sim 3 \text{ nm}$ , which suggests that the surface may play an important role in stabilizing this final stage. It is evident in Fig. 6 that the regrowth rate during the second stage increases with increasing beam flux over the range from  $1.2$  to  $5.0 \times 10^{20} \text{ cm}^{-2} \text{ s}^{-1}$ , but shows no further increase with increasing flux above  $5.0 \times 10^{20} \text{ cm}^{-2} \text{ s}^{-1}$ .

Thermal and irradiation-enhanced recrystallization are separate processes, and the regrowth rate,  $V(T)$ , at the *a/c* interface can be described as<sup>27</sup>

$$V(T) = V_{\text{irr}} \exp(-E_{\text{irr}}/kT) + V_{\text{th}} \exp(-E_{\text{th}}/kT), \quad (7)$$

where  $k$  is the Boltzmann constant,  $E_{\text{irr}}$  and  $E_{\text{th}}$  are activation energies, and  $V_{\text{irr}}$  and  $V_{\text{th}}$  are prefactors for irradiation-enhanced and thermal epitaxial processes, respectively. A few thermal epitaxial regrowth regimes have been previously observed in  $\text{SrTiO}_3$  with activation energies of 0.77 eV in air,<sup>37</sup> 1.21 eV in  $\text{N}_2$ ,<sup>38</sup> and 2.14 eV in vacuum,<sup>36</sup> as summarized in Fig. 7 as dashed lines. The two data points on each line indicate the lower and upper temperature limits for the corresponding studies.<sup>36–38</sup> In order to compare the thermal regrowth rates with the current data, the fitted lines are extrapolated to lower temperatures. The extrapolated lines indicate that all these thermal regrowth mechanisms will be negligible below 400 K, especially for the case of thermal annealing in vacuum, which is the most similar to the conditions of the present study. The recrystallization rates under

e-beam irradiation at ion fluxes of  $2.8$  and  $5.0 \times 10^{20} \text{ cm}^{-2} \text{ s}^{-1}$  were measured by TEM observation at three different temperatures, as shown in Fig. 7. The significantly higher recrystallization rates at these temperatures under different e-beam fluxes indicate that the recrystallization processes at the *a/c* interface are primarily attributed to e-beam enhanced recrystallization processes rather than thermal regrowth processes. Since thermal regrowth is insignificant at temperature below  $400 \text{ K}$ , only the irradiation term in Eq. (7) is fit to the data from this study, which yields values of  $E_{\text{irr}}=0.11 \text{ eV}$  and  $V_{\text{irr}}=0.7 \text{ nm s}^{-1}$  for an e-beam flux of  $2.8 \times 10^{20} \text{ cm}^{-2} \text{ s}^{-1}$ , and  $E_{\text{irr}}=0.10 \text{ eV}$  and  $V_{\text{irr}}=0.9 \text{ nm s}^{-1}$  for a flux of  $5.0 \times 10^{20} \text{ cm}^{-2} \text{ s}^{-1}$ . Considering the uncertainty in the TEM measurements, the activation energy for recrystallization under e-beam irradiation is  $0.10 \pm 0.05 \text{ eV}$ , which is significantly lower than the thermal activation energies previously reported.<sup>36–38</sup> By extrapolating the line fits of the data for e-beam enhanced recrystallization to the temperature regime of thermal annealing in vacuum, the results in Fig. 7 indicate that both recrystallization processes are important in the temperature regime between  $600$  and  $700 \text{ K}$ . As temperature increases above  $700 \text{ K}$ , thermal epitaxial regrowth processes will be dominant. It is interesting to note that the solid phase regrowth in Fig. 6 shows a sublinearlike dependence on exposure time to the e-beam. Since superlinearlike behavior is normally observed in thermal recrystallization,<sup>17,37</sup> this different feature may be used as a fingerprint between the two recrystallization mechanisms.

Ion-beam-induced epitaxial crystallization (IBIEC) (Refs. 3, 11, and 53) has been investigated for many years, and most of the proposed models assume that migration of irradiation-induced defects are the dominant contribution to IBIEC. In the current study of e-beam irradiation, the recrystallization is attributed solely to relaxation process at the *a/c* interface due to the electron energy deposition, rather than indistinguishable processes from nuclear stopping and electronic stopping under ion irradiation. Moreover, the well-controlled TEM technique applied in this study provides direct *in situ* observation of the regrowth processes, which has advantages over ion beam techniques, such as RBS that may induce additional IBIEC effects during ion beam analysis. Previous photoluminescence measurements<sup>24</sup> have indicated that room temperature electron irradiation of  $\text{SrTiO}_3$  at energies from  $200$  to  $600 \text{ keV}$  causes negligible permanent defects. Thus, the mechanism for significant e-beam enhanced recrystallization during the second stage is unlikely due to defect production and annihilation. During e-beam irradiation,

the incident electrons primarily transfer energy by ionization processes that produce localized electronic excitations. The localized electronic excitations affect local atomic bonds and may effectively lower the energy barriers to defect recovery and recrystallization processes, which may involve local atomic hopping or rotation of atomic polyhedra. While ion-beam induced defects may contribute to the irradiation-enhanced recovery observed under Au irradiation (Figs. 1, 3, and 4), the present electron beam results suggest that ionization-enhanced recovery may also play a role.

#### IV. CONCLUSIONS

Damage accumulation behavior in single crystals  $\text{SrTiO}_3$  under Au irradiation were studied over temperatures from  $150$  to  $400 \text{ K}$ . The results show similar disordering behavior on both Sr and Ti sublattices, where the atomic disorder increases nonlinearly with dose until a fully amorphous state is achieved. The nonlinear damage evolution at and below  $360 \text{ K}$  can be described by a disorder accumulation model indicating that the defect-stimulated amorphization is the dominant mechanism leading to amorphization in  $\text{SrTiO}_3$ . Significant dynamic recovery of the ion-induced damage occurs as the irradiation temperature increases, and the rate of damage accumulation decreases dramatically at higher temperatures. The critical temperature for amorphization in  $\text{SrTiO}_3$  is about  $370 \text{ K}$  under these irradiation and analysis conditions, which is in good agreement with previous *in situ* TEM results. The damage accumulation kinetics is consistent with irradiation-enhanced and thermal recovery processes with activation energies of  $0.1 \pm 0.05$  and  $0.7 \pm 0.1 \text{ eV}$ , respectively. The current study also demonstrates that the e-beam induced recrystallization of amorphous  $\text{SrTiO}_3$  occurs through epitaxial regrowth at the *a/c* interface. The regrowth rate is several orders magnitudes higher than the thermal epitaxial growth over the same temperature range. The activation energy for e-beam enhanced recrystallization is  $0.10 \pm 0.05 \text{ eV}$ . The fast recrystallization may be attributed to localized electronic excitations that lower energy barriers for rearrangement of interfacial atoms.

#### ACKNOWLEDGMENTS

This work was supported by the Division of Materials Science and Engineering, Office of Basic Energy Sciences, U.S. Department of Energy under Contract No. DE-AC05-76RL01830 (PNNL) and Grant No. DE-FG02-97ER45656 (UM). The operational support for the EMSL accelerator was provided by the Office of Biological and Environmental Research, U.S. Department of Energy.

\*Author to whom correspondence should be addressed. Mailing address: Pacific Northwest National Laboratory, P.O. Box 999/MS K8-93, Richland, Washington 99352. Electronic address: Yanwen.Zhang@pnl.gov

<sup>1</sup>N. Erdman, K. R. Poeppelmeler, M. Asta, O. Warschkow, D. E. Ellis, and L. D. Marks, *Nature (London)* **419**, 55 (2002).

<sup>2</sup>G. D. Wilk, R. M. Wallace, and J. M. Anthony, *J. Appl. Phys.* **89**,

5243 (2001).

<sup>3</sup>K. Oyoshi, S. Hishita, and H. Haneda, *J. Appl. Phys.* **87**, 3450 (2000).

<sup>4</sup>M. Kiyotoshi and E. Kazuhiro, *Appl. Phys. Lett.* **67**, 2468 (1995).

<sup>5</sup>S. L. Swartz, *IEEE Trans. Electr. Insul.* **25**, 935 (1990).

<sup>6</sup>C. Aruta, *Phys. Status Solidi A* **183**, 353 (2001).

<sup>7</sup>A. Kosola, M. Putkonen, L.-S. Johansson, and L. Niinistö, *Appl.*

- Surf. Sci. **211**, 102 (2003).
- <sup>8</sup>W. J. Weber, R. C. Ewing, C. R. A. Catlow, T. Diaz de la Rubia, L. W. Hobbs, C. Kinoshita, H. J. Matzke, A. T. Motta, M. Nastasi, E. K. H. Salje, E. R. Vance, and S. J. Zinkle, *J. Mater. Res.* **13**, 1434 (1998).
- <sup>9</sup>A. E. Ringwood, S. E. Kesson, K. D. Reeve, D. M. Levins, and E. J. Ramm, in *Radioactive Waste Forms for the Future*, edited by W. Lutze and R. C. Ewing (North-Holland, Amsterdam, 1988), p. 233.
- <sup>10</sup>R. C. Ewing, W. J. Weber, and J. Lian, *J. Appl. Phys.* **95**, 5949 (2004).
- <sup>11</sup>S. Nakao, Z. Wang, P. Jin, Y. Miyagawa, and S. Miyagawa, *Nucl. Instrum. Methods Phys. Res. B* **191**, 226 (2002).
- <sup>12</sup>J. Albrecht, S. Leonhardt, R. Spolenak, U. Täffner, H.-U. Habermeyer, and G. Schütz, *Surf. Sci.* **547**, 847 (2003).
- <sup>13</sup>A. Meldrum, L. A. Boatner, and R. C. Ewing, *Nucl. Instrum. Methods Phys. Res. B* **141**, 347 (1998).
- <sup>14</sup>A. Meldrum, L. A. Boatner, W. J. Weber, and R. C. Ewing, *J. Nucl. Mater.* **300**, 242 (2002).
- <sup>15</sup>C. Sabathier, J. Chaumont, and J.-C. Krupa, *Nucl. Instrum. Methods Phys. Res. B* **196**, 308 (2002).
- <sup>16</sup>C. W. White, C. J. McHargue, P. S. Sklad, L. A. Boatner, and G. C. Farlow, *Mater. Sci. Rep.* **4**, 41 (1989).
- <sup>17</sup>J. Rankin, B. W. Sheldon, and L. A. Boatner, *J. Mater. Res.* **9**, 3113 (1994).
- <sup>18</sup>W. J. Weber, W. Jiang, S. Thevuthasan, R. E. Williford, A. Meldrum, and L. A. Boatner, *Defects and Surface-Induced Effects in Advanced Perovskites*, edited by G. Borstel (Kluwer Academic, The Netherlands, 2000), p. 317.
- <sup>19</sup>Y. Zhang, W. J. Weber, W. Jiang, A. Hallén, and G. Possnert, *J. Appl. Phys.* **91**, 6388 (2002).
- <sup>20</sup>Y. Zhang, W. J. Weber, W. Jiang, C. M. Wang, V. Shutthanandan, and A. Hallén, *J. Appl. Phys.* **95**, 4012 (2004).
- <sup>21</sup>W. Chu, J. W. Mayer, and M. Nicolet, *Backscattering Spectrometry* (New York San Francisco, London, 1978).
- <sup>22</sup>J. F. Ziegler, J. P. Biersack, and U. Littmark, *The Stopping and Range of Ions in Solids* (Pergamon, New York, 1985).
- <sup>23</sup>J. F. Ziegler, SRIM-2000, v. 2000.40, <http://www.srim.org>.
- <sup>24</sup>R. Cooper, K. L. Smith, M. Colella, E. R. Vance, and M. Phillips, *J. Nucl. Mater.* **289**, 199 (2001).
- <sup>25</sup>K. L. Smith, M. Colella, R. Cooper, and E. R. Vance, *J. Nucl. Mater.* **321**, 19 (2003).
- <sup>26</sup>K. L. Smith and N. J. Zaluzec, *J. Nucl. Mater.* **336**, 261 (2005).
- <sup>27</sup>W. J. Weber, *Nucl. Instrum. Methods Phys. Res. B* **166-167**, 98 (2000).
- <sup>28</sup>N. Hecking, K. F. Heidemann, and E. TE Kaat, *Nucl. Instrum. Methods Phys. Res. B* **15**, 760 (1986).
- <sup>29</sup>W. J. Weber, *J. Nucl. Mater.* **98**, 206 (1981).
- <sup>30</sup>M. L. Swanson, *Handbook of Modern Ion Beam Materials Analysis*, edited by J. R. Tesmer and M. Nastasi (Materials Research Society, Pittsburgh, PA, 1995), p. 263.
- <sup>31</sup>J. S. Williams and R. G. Elliman, *Ion Beams for Materials Analysis*, edited by J. R. Bird and J. S. Williams (Academic, Australia, 1989), p. 286.
- <sup>32</sup>L. C. Feldman, J. W. Mayer, and S. T. Picraux, *Materials Analysis by Ion Channeling* (Academic, New York, 1982), p. 117.
- <sup>33</sup>Y. Zhang, F. Gao, W. Jiang, D. E. McCready, and W. J. Weber, *Phys. Rev. B* **70**, 125203 (2004).
- <sup>34</sup>Y. Zhang, W. J. Weber, V. Shutthanandan, R. Devanathan, S. Thevuthasan, G. Balakrishnan, and D. M. Paul, *J. Appl. Phys.* **95**, 2866 (2004).
- <sup>35</sup>M. J. Akhtar, Z. Akhtar, R. A. Jackson, and C. R. A. Catlow, *J. Am. Ceram. Soc.* **78**, 421 (1995).
- <sup>36</sup>T. W. Simpson, I. V. Mitchell, J. C. McCallum, and L. A. Boatner, *J. Appl. Phys.* **76**, 2711 (1994).
- <sup>37</sup>C. W. White, L. A. Boatner, P. S. Sklad, C. J. McHargue, J. Rankin, G. C. Farlow, and M. J. Aziz, *Nucl. Instrum. Methods Phys. Res. B* **32**, 11 (1988).
- <sup>38</sup>J. C. McCallum, J. Rankin, C. W. White, and L. A. Boatner, *Nucl. Instrum. Methods Phys. Res. B* **46**, 98 (1990).
- <sup>39</sup>J. Rankin, J. C. McCallum, and L. A. Boatner, *J. Appl. Phys.* **73**, 1519 (1995).
- <sup>40</sup>J. Rankin, J. C. McCallum, and L. A. Boatner, *J. Mater. Res.* **7**, 717 (1992).
- <sup>41</sup>A. Meldrum, L. A. Boatner, and R. C. Ewing, *J. Mater. Res.* **12**, 1816 (1997).
- <sup>42</sup>S. H. Nam and H. G. Kim, *J. Appl. Phys.* **72**, 2895 (1992).
- <sup>43</sup>Y. Zhang, W. J. Weber, W. Jiang, V. Shutthanandan, S. Thevuthasan, M. Janson, and A. Hallén, *Nucl. Instrum. Methods Phys. Res. B* **219-220**, 647 (2004).
- <sup>44</sup>K. Szot and W. Speier, *Phys. Rev. B* **60**, 5909 (1999).
- <sup>45</sup>M. O. Ruault, J. Chaumont, J. M. Pennison, and A. Bourret, *Philos. Mag. A* **50**, 667 (1984).
- <sup>46</sup>G. Lulli, P. G. Merli, and M. V. Antisari, *Phys. Rev. B* **36**, 8038 (1987).
- <sup>47</sup>L. M. Wang and W. J. Weber, *Philos. Mag. A* **79**, 237 (1999).
- <sup>48</sup>S. B. Fisher, *Radiat. Eff.* **5**, 239 (1970).
- <sup>49</sup>I. Jenčič, M. W. Bench, I. M. Robertson, and M. A. Kirk, *J. Appl. Phys.* **78**, 974 (1995).
- <sup>50</sup>*Chemical Rubber Company Handbook of Chemistry and Physics*, edited by D. R. Lide, 79th ed. (CRC Press, Boca Raton, 1998).
- <sup>51</sup>ICRU Report 37, International Commission on Radiation Units and Measurements, Stopping Powers for Electrons and Positrons, ICRU (1984).
- <sup>52</sup>I. G. Salisbury, R. S. Timsit, S. D. Berger, and C. J. Humphreys, *Appl. Phys. Lett.* **45**, 1289 (1984).
- <sup>53</sup>F. Priolo and E. Rimini, *Mater. Sci. Rep.* **5**, 319 (1990).